Compact LED-based full-field optical coherence microscopy for high-resolution high-speed in vivo imaging

Jonas Ogien, Arnaud Dubois

Compact LED-based full-field optical coherence microscopy for high-resolution high-speed *in vivo* imaging

Jonas Ogien*[a], Arnaud Dubois[a]
[a]Laboratoire Charles Fabry, CNRS UMR 8501, Institut d'Optique Graduate School, Univ. Paris-Sud, 2 avenue Augustin Fresnel, 91127 Palaiseau Cedex, France

ABSTRACT

This work reports on a compact full-field optical coherence microscopy (FF-OCM) setup specifically designed to meet the needs for *in vivo* imaging, illuminated by a high-brightness broadband light emitting diode (LED). Broadband LEDs have spectra potentially large enough to provide imaging spatial resolutions similar to those reached using conventional halogen lamps, but their radiance can be much higher, which leads to high speed acquisition and makes *in vivo* imaging possible. We introduce a FF-OCM setup using a 2.3 W broadband LED, with an interferometer designed to be as compact as possible in order to provide the basis for a portable system that will make it possible to fully benefit from the capacity for *in vivo* imaging by providing the ability to image any region of interest in real-time. The interferometer part of the compact FF-OCM setup weighs 210 g for a size of 11×11×5 cm^3. Using this setup, a sub-micron axial resolution was reached, with a detection sensitivity of 68 dB at an imaging rate of 250 Hz. Due to the high imaging rate, the sensitivity could be improved by accumulation while maintaining an acquisition time short enough for *in vivo* imaging. It was possible to reach a sensitivity of 75 dB at a 50 Hz imaging rate. High resolution *in vivo* human skin images were obtained with this setup and compared with images of excised human skin, showing high similarity.

Keywords: Optical coherence tomography, medical and biological imaging, interference microscopy.

1. INTRODUCTION

Optical Coherence Tomography (OCT) is a low coherence interferometric imaging technique capable of vertical cross-sectional imaging of biological tissues with micrometer scale resolution in a non invasive way[1]. It has initially drawn much attention in the field of ophthalmology[2] where it has been established as the gold standard for retinal imaging in a remarkably short amount of time, as it constitutes a powerful tool for monitoring retinal layers morphology in real-time, *in vivo*. OCT has also seen much interest in the field of dermatology[3], nevertheless, in conventional frequency domain (FD) OCT, the lateral resolution is limited by the depth of focus of the system, which must be large enough to match at least the penetration depth as there is conventionally no refocusing process. This constitutes a limitation for dermatological imaging were cellular-level imaging is often of importance.

Full-Field Optical Coherence Microscopy (FF-OCM), also referred to as Full-Field OCT (FF-OCT) is a parallelized approach of OCT where *en face* images are recorded using an area sensor and full-field illumination[4-10]. In *en face* imaging, there is no depth of field constraint as the image is obtained in a given plane, and therefore microscope objectives of higher numerical apertures (NA) can be used to achieve higher transverse resolution. Cellular level imaging within the skin is therefore achievable and FF-OCM has seen developments oriented towards dermatological imaging[11,12]. Nevertheless, contrary to FD-OCT where acquisition of the interferometric data is very fast due to the development of high-speed swept-source lasers, FF-OCM speed is generally a limiting factor regarding *in vivo* imaging. Up to now, there have been several efforts to make *in vivo* imaging feasible with FF-OCM by improving imaging speed. Implementations of *in vivo* FF-OCM included the use of single-shot setups using two cameras, or the use of high brightness light sources in order to yield fast acquisition of the interferometric data, and sometimes a combination of those two methods[13-21]. Nevertheless, owing to the fact that some of those implementations have been done at the price of a loss of image quality and that most of them are complex and/or expensive, *in vivo* imaging is still not a common feature of FF-OCM.

*jonas.ogien@institutoptique.fr; phone +331.64.53.32.71

This paper introduces a simple and inexpensive FF-OCM setup designed for *in vivo* imaging, based upon a Linnik interference microscope and using a single camera. A high-brightness broadband light emitting diode (LED) is employed as the light source for high speed and high spatial resolution imaging. Furthermore, an innovative and compact design is introduced in order to provide the basis for a portable system which will properly meet the needs for *in vivo* imaging, that is to easily image any region of interest in real-time. The setup is characterized in terms of axial and transverse resolutions, detection sensitivity and operation speed. Application of the setup for biomedical imaging is then investigated by imaging human skin *in vivo* and *ex vivo*.

2. HIGH-SPEED IMAGING WITH FF-OCM

The imaging speed in FF-OCM is mainly determined by several factors: radiance of the light source, full well capacity (FWC) of the camera sensor, and number of interferometric images needed in order to reconstruct an *en face* tomographic image.

2.1 Radiance and FWC

In FF-OCM, in order to obtain the best possible imaging sensitivity for a given camera sensor, it is necessary that its pixels FWC is almost completely filled during image acquisition (*i.e.* the pixels are close to saturation). As sensitivity is a critical parameter, cameras with large FWC (*i.e* high dynamic cameras) should be used in FF-OCM for biomedical imaging, in order to reach sensitivities high enough to image very low reflecting features within biological tissues. Therefore, the time required to record one image (the integration time of the camera) with filled FWC is directly linked to the irradiance upon the camera sensor. The higher it is, the faster the FWC is filled, and the faster imaging is, with no loss regarding sensitivity. Irradiance upon the camera sensor being linked to the radiance of the light source according to Eq. (1) considering a simple approximation where the radiance is uniform, with E being the irradiance in the sensor plane, K being the percentage of the spectrum of emission of the light source actually detected by the sensor (considering its quantum efficiency, and losses within the optical system), L being the radiance of the light source, G being the limiting geometrical extent of the optical system, and A being the area illuminated over the sensor plane (considered uniform as the radiance is uniform):

$$E = \frac{KG}{A} L \tag{1}$$

For a given FF-OCM system, the higher the radiance of the light source, the faster the system can acquire interferometric data. Note that it is often difficult to reach very low integration times in FF-OCM as, by principle, the whole field to be imaged is illuminated, meaning that A takes rather large values in Eq. (1), and spatially incoherent light sources must be used in order to avoid artifacts[22], generally resulting in low radiance values.

If the sample moves during the acquisition of the interferometric data (especially axially, as the phase rapidly varies in that direction), the recorded interference fringes can quickly be washed out if the integration time is too high[20], resulting in a loss of signal. Considering *in vivo* imaging, it is essential that the integration time is low enough to avoid any fringe washout due to movements of the subject being imaged, especially if a system capable of *in vivo* imaging in common conditions with no particular means of subject stabilization (such as physical constraint or anesthesia) is desired.

2.2 Reconstruction of tomographic images

In FF-OCM, the tomographic images are the result of a combination of several phase-shifted interferometric images according to a given demodulation algorithm. Consequently, the time needed to acquire a tomographic image is at least the integration time multiplied by the number of interferometric images needed by the demodulation algorithm being used. In practice, time is also needed for the camera to transfer the data read by all the pixels during its integration time. The overall time needed to acquire the data and transfer it is referred to as the frame time of the camera, and thus the time needed to acquire a tomographic image is the frame time multiplied by the number of interferometric images needed for reconstruction. It should be noted that even though the integration time of the camera can be reduced by increasing the radiance of the light source, the actual frame time of the camera cannot always be reduced accordingly. Nevertheless, with some cameras, it is possible to define the number of pixels actually in use, and decreasing that

number can reduce the frame time, as there is less information to be transferred, at the price of smaller fields being imaged or a loss in spatial resolution.
Another process that can affect the speed of acquisition of tomographic images is image accumulation. Before applying the demodulation algorithm, several interferometric images corresponding to the same applied phase-shift are summed up in order to boost the interferometric signal. This increases the detection sensitivity according to Eq. (2), with S_0 being the sensitivity when no image accumulation is performed, and N being the number of images that are accumulated:

$$S = S_0 + 10\log_{10}(N) \quad (2)$$

At the same time, the acquisition time is multiplied by N. Image accumulation is almost always performed in FF-OCM when high quality images are desired.

Therefore, the total time to acquire a single tomographic image is the frame time multiplied by the number of images needed by the reconstruction algorithm multiplied by the number of images accumulated for each phase-shift. Note that at least three images are needed for reconstruction in order to properly demodulate the interferometric data.

Hence, even for a system for which the integration time is very low, the actual time to record a tomographic image may be significantly higher. In order to reduce it as much as possible, a two-image algorithm can be used[23]. Although a two-image algorithm cannot demodulate the interferometric signal (it just removes the signal background), it still gives good results regarding imaging biological samples. As mentioned previously, single shot setups, which are generally complex and costly, have also been proposed[17-21].

Regarding *in vivo* imaging, it should be noted that movement of the subject between successive interferometric images is less critical than during the acquisition of the interferometric data. As long as the interferometric signal has been acquired, movements between images used for reconstruction can only result in artifacts due to the recombination of signals corresponding to different zones of the subject due to its movement, that generate interferometric signals with different amplitudes[20]. As the amplitude varies much more slowly than the phase (an error in the phase will generally not greatly affect the quality of demodulation, some algorithms insensitive to phase errors have even been developed), the constraint regarding movement over the total acquisition time is less severe than over the integration time of the camera. Nevertheless, those artifacts can significantly affect the quality of the images and should be minimized.

3. EXPERIMENTAL SETUP

The high speed, high resolution FF-OCM setup reported here is based on a Linnik interference microscope, the configuration that has been the most widely used in FF-OCM[5-9]. It consists of a Michelson interferometer with a microscope objective in each arm, providing high transverse resolution and magnification. It has the advantage of providing flexibility regarding the choice of numerical aperture (NA) and immersion medium, while reducing light losses compared to the Mirau or Michelson interference microscope configurations, a fundamental point when high imaging speed is targeted. In order to optimize *in vivo* imaging, the interferometer was designed to be as compact as possible, with the aim to lay the foundations for a handheld system, as the capacity for *in vivo* imaging is of greater interest if it is possible to image in real-time any region of interest. Furthermore, a compact system limits motion artifacts due to external vibrations.

The designed interferometer consists in two identical microscope objectives (10x, NA = 0.3, water-immersion, Olympus) and a cube beamsplitter as small as possible, with the objectives directly connected to the beamsplitter cube housing, resulting in an interferometer with very short arms, having a total size of 11×11×5 cm^3 and weighing 210 g, making it suitable for a future compact and light handheld setup. Silicone oil, whose refractive index typically matches the one of biological tissues, is used as immersion liquid to compensate for optical dispersion. In the object arm, the objective rests within a tank full of immersion liquid at the bottom of which a glass plate (0.5-mm-thick, made of fused silica) was placed to enable imaging the sample through it, while also permitting to press the sample against it in order to limitate sample motion as much as possible. In the reference arm, a tank full of immersion liquid is directly linked to the objective. A similar glass plate is placed at the bottom of the tank in order to compensate for the optical dispersion introduced by the plate in the object arm while also providing a 3.5% reflectivity reference surface (interface between glass and air) appropriate for FF-OCM imaging. This glass plate serving as a reference surface was placed upon a small piezoelectric (PZT) chip (5.0×5.0×2.4 mm^3) included within the tank, that is used for providing phase shifting in order to

demodulate the interferometric signal, while the whole interferometer is placed upon a PZT stage used to set the imaging depth, and enable three-dimensional imaging. Figure 1 shows a schematic of the setup.

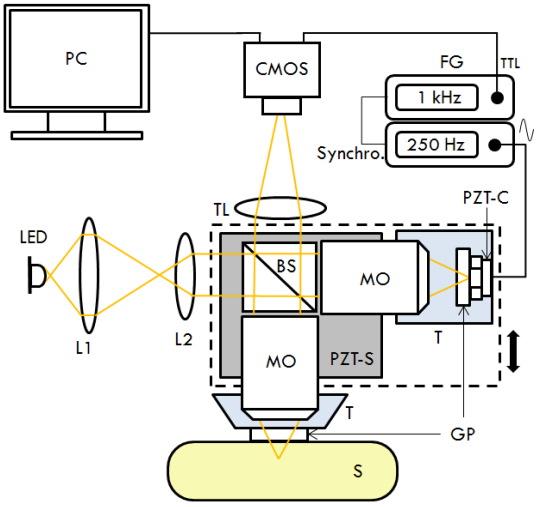

Figure 1. Schematic representation of the compact FF-OCM setup. L1, collector lens; L2, condenser lens; BS, beam-splitter; MO, microscope objectives; T, tanks containing silicone oil; GP, glass plates; S, sample; PZT-C, piezoelectric chip; PZT-S, piezoelectric stage; TL, tube lens; CMOS, complementary metal oxide semi-conductor camera; FG, function generator; TTL, transistor-transistor logic; PC, personal computer. The dashed rectangle represents the part of the interferometer moving vertically due to PZT S.

In order to maximize the speed of the imaging system, we introduce the use of a high brightness broadband LED as the light source. Currently, phosphor LEDs having broad spectra and high radiant fluxes are starting to be commercially available. Recently, the use of a broadband LED for FF-OCM has been shown to yield identical images compared to those obtained with a conventional halogen lamp[24], nevertheless, the radiant flux of the LED was not high enough for high-speed imaging. The LED used in the present setup has a 2.3 W radiant flux, with a spectrum having a FWHM of 145 nm and a central wavelength of 600 nm, yielding an axial resolution for FF-OCM of 0.9 µm, as shown in Fig. 2. It should be noted that the spectrum is not optimal for penetration in biological tissues, as it spans over only a small part of the optical therapeutic window. Nevertheless, penetration up to a few hundreds microns is still possible. Considering the LED directivity (125° viewing angle), size (12.25 mm²) and radiant flux, it is possible to estimate its radiance to be 70 $mW.m^{-2}.str^{-1}$. By comparison, a typical radiance with a high-brightness halogen lamp is 10 $mW.m^{-2}.str^{-1}$. The LED-based setup can achieve image rates up to 7 times superior to conventional halogen lamp based setups, if the same camera is used. Therefore this LED-based setup provides a high-speed acquisition while maintaining a high resolution, and benefits from the numerous advantages of LED illumination, including compactness, low power consumption, ease of use and maintenance, and long lifetime.

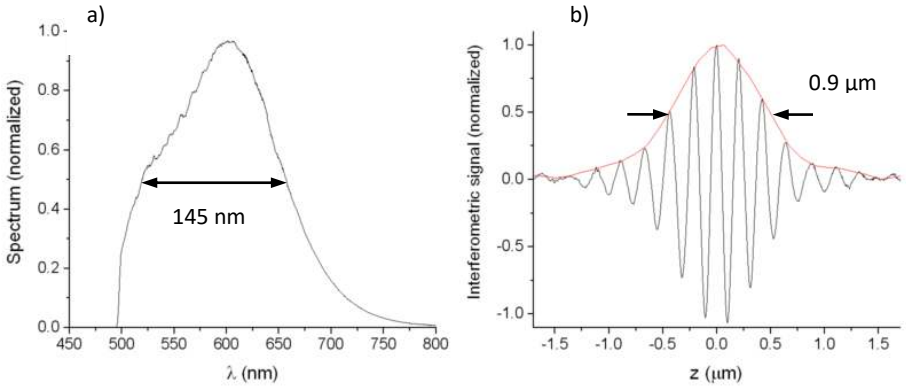

Figure 2. a) Spectrum of the LED light source. An interference filter was used to filter out the blue component of the spectrum; b) Axial interferometric response of the system, that determines the imaging axial resolution.

As explained above, in order to benefit from the high LED radiance, the camera must also have a high frame rate (and a high FWC for high sensitivity). A CMOS camera (Photonfocus, model MV1-D1026E-160-CL) with a FWC of 200,000 e^-, was used. The frame rate of the camera can be significantly increased by limiting its number of pixels in use. Considering our LED, the integration time of the camera could be as low as 920 µs while maintaining the pixels close to saturation, resulting in a measured detection sensitivity of 68 dB. Nevertheless, the frame time was limited to ~ 7 ms if all the pixels (1024×1024) were in use. In order to reduce the frame time to be as close as possible to the integration time while maintaining a relevant field of view (above 200x200 µm²), 250×250 pixels were used, resulting in a FOV of 250×250 µm², and a frame rate of up to 1000 frames per seconds (fps). A four-frame algorithm with sinusoidal phase modulation was used for demodulation[25], yielding an FF-OCM imaging rate of 250 Hz. This rate enables *in vivo* imaging by significantly limiting motion artifacts, as explained in section 2. In order to further improve the sensitivity, it was even possible to perform image accumulation with five interferometric images while keeping *in vivo* imaging feasible. The resulting sensitivity was then boosted to 75 Hz, as shown in Figure 3. Experiments shown that past this number of accumulated images, no significant gain in image quality was obtained, as the gain in sensitivity was then counterbalanced by image degradation due to artifacts linked to the increased in acquisition time. With five images accumulated, the imaging rate was 50 Hz. In order to increase the signal to noise ratio of the images obtained even further, every five images were averaged together, resulting in a 10 Hz imaging rate, which can still be considered as video rate. Note that this last averaging is done after the tomographic images have been obtained, and therefore no signal can be lost during this step. Motion can just cause a blurring of the image if it is too significant during the acquisition of the five tomographic images to be averaged together.

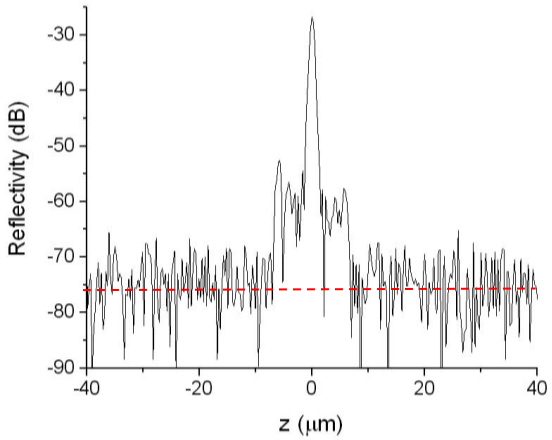

Figure 3. Axial response of the FF-OCM system in logarithm scale, with five images accumulated. The dashed line indicates the detection sensitivity of the system.

4. RESULTS

In order to show the ability of this FF-OCM setup to produce images *in vivo* with no loss in resolution or sensitivity compared to images of immobile samples, imaging of human skin both *in vivo* and *ex vivo* was performed. *In vivo* skin imaging is one of the main goals of FF-OCM in order to make this imaging technique more widely used in a clinical context[11,26].

The *ex vivo* sample consisted of healthy human skin excised from the neck region. *In vivo* measurements were carried out on the author's hand. The imaging procedure consisted in pressing the skin onto the glass plate of the interferometer object arm as described above, after having placed a drop of dermatoscopy oil onto the skin in order to attenuate the reflection of the glass plate. Tomographic images were displayed in real time at a 10 Hz rate using a custom C++ software. Using the PZT stage, images could be obtained at several axial positions of interest within the epidermis. It was possible to penetrate roughly up to the superficial dermis, about 150 µm in depth. Images obtained within the stratum granulosum, stratum spinosum, and stratum basale are presented in Figure 4. A slight Gaussian blur was applied on the images for display in this paper.

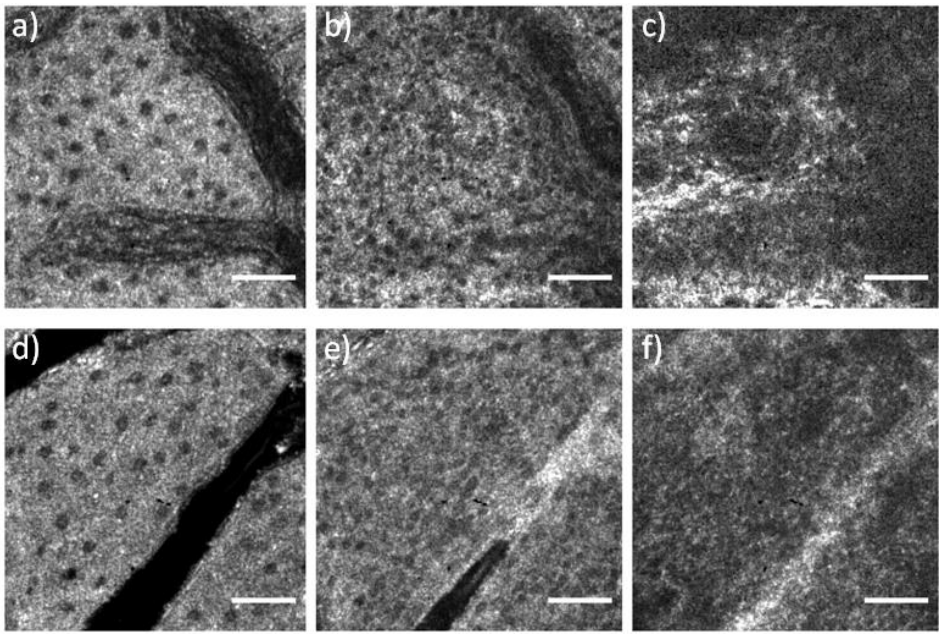

Figure 4. Images of human skin obtained with the FF-OCM setup; a) b) and c) : *in vivo*, within the stratum granulosum, stratum spinosum and stratum basale, respectively; d), e) and f) : *ex vivo*, within the same layers, respectively. Scale bars are 50 µm.

It should be noted that the skin imaged *in vivo* originated from a different location within the body than skin imaged *ex vivo*, resulting in some differences regarding the structure of the skin. Nevertheless, cellular level imaging is clearly demonstrated both *in vivo* and *ex vivo*, and the images are highly similar, showing that the image acquisition is rapid enough for the motion of the subject not to affect image quality. It should be emphasized that the subject being imaged was just pressing his skin onto the glass plate, with no other means of stabilization.

5. CONCLUSION

This work presents the implementation of a compact FF-OCM setup specifically designed to meet the needs for *in vivo* imaging, illuminated by a high-brightness broadband LED. This setup constitutes a simple implementation of FF-OCM, using a common demodulation process, common Linnik configuration and an inexpensive and easy to use light source, which provides high resolution *in vivo* imaging. It constitutes a proof of principle that *in vivo* imaging is possible in FF-OCM without having to resort to any complex method. Furthermore, the compactness of the introduced design paves the way for portable FF-OCM setups that will make it possible fully benefit from the capacity of FF-OCM for *in vivo* imaging, especially in a clinical context.

This work also constitutes a step towards the advent of LED illumination in FF-OCM, as it is shown that the high radiance of LED combined with a broad spectrum enables image rates superior to conventional thermal-light illumination, while maintaining a similar spatial resolution, and benefiting from the numerous advantages of LED illumination.

Currently, the main limitation of the system concerns the camera. Even though it is possible to reach short integration times using the LED, the frame time of the camera cannot be reduced accordingly if all of its pixels are used, impeding large field imaging. Furthermore the FWC of our camera is not high enough for high quality imaging without image accumulation, which is also a limiting factor. Those limitations could be overcome by the availability of more appropriate cameras in order to benefit from the full potential of LED illumination for high-speed FF-OCM.

REFERENCES

[1] Huang, D., Swanson, E. A., Lin, C. P., Schuman, J. S., Stinson, W. G., Chang, W., Hee, M. R., Flotte, T., Gregory, K., Puliafito, C. A. and Fujimoto, J. G., "Optical coherence tomography," Science 254, 1178-1181 (1991).

[2] Swanson, E. A., Izatt, J. A., Hee, M. R., Huang, D., Lin, C. P., Schuman, J. S., Puliafito, C. A. and Fujimoto, J. G., "In vivo retinal imaging by optical coherence tomography," Opt. Lett. 18, 1864-1866 (1993).

[3] Welzel, J., "Optical coherence tomography in dermatology: a review, " Skin Research & Tech. 7, 1-9 (2001).

[4] Beaurepaire, E., Boccara, A. C., Lebec, M., Blanchot, L., Saint-Jalmes, H., "Full-field optical coherence microscopy," Opt. Lett. 23, 244–246. (1998)

[5] Vabre, L., Dubois, A. and Boccara, A.C., "Thermal-light full-field optical coherence tomography," Opt. Lett., 27, 530-532 (2002)

[6] Dubois, A., Vabre, L., Boccara A.C. and Beaurepaire, E., "High-resolution full-field optical coherence tomography with a Linnik microscope,"Appl. Opt. 41, 805-812 (2002).

[7] Dubois, A., Grieve, K., Moneron, G., Lecaque, R., Vabre, L. and Boccara, A.C., "Ultrahigh-resolution full-field optical coherence tomography," Appl. Opt. 43, 2874-2882 (2004).

[8] Oh, W. Y., Bouma, B. E., Iftimia, N., Yun, S. H., Yelin, R. and Tearney, G. J., "Ultrahigh-resolution full-field optical coherence microscopy using InGaAs camera," Opt. Express 14, 726-735 (2006).

[9] Dubois, A., Moneron, G. and Boccara, C., "Thermal-light full-field optical coherence tomography in the 1.2μm wavelength region," Opt. Commun. 266, 738-743 (2006).

[10] Dubois, A., [Handbook of full-field optical coherence microscopy: technology and applications], Pan Stanford Publishing, Singapore (2016).

[11] Dalimier, E. and Salomon, D., "Full-Field Optical Coherence Tomography: A New Technology for 3D High-Resolution Skin Imaging, " Dermatology 224, 84-92 (2012).

[12] Tsai, C.-C., Chang, C.-K., Hsu, K.-Y., Ho, T.-S., Lin, M.-Y., Tjiu, J.-W. and Huang S.-L., "Full-depth epidermis tomography using a Mirau-based full-field optical coherence tomography," Biomed. Opt. Express 5, 3001-3010 (2014).

[13] Akiba, M. and Chan, K. P., "In vivo video-rate cellular-level full-field optical coherence tomography," J. Biomed. Opt. 12, 064024 (2007).

[14] Subhash, H.M., "Full-Field and Single-Shot Full-Field Optical Coherence Tomography: A Novel Technique for Biomedical Imaging Applications, " Advances in Optical Technologies 2012, 435408 (2012)

[15] Latrive, A. and Boccara, A. C., "In vivo and in situ cellular imaging full-field optical coherence tomography with a rigid endoscopic probe," Biomed. Opt. Express 2, 2897-2904 (2011).

[16] Grieve, K., Dubois, A., Simonutti, M., Paques, M., Sahel, J., Le Gargasson, J.-F. and Boccara, A. C., "In vivo anterior segment imaging in the rat eye with high speed white light full-field optical coherence tomography," Opt. Express 13, 6286-6295 (2005).

[17] Moneron, G., Boccara, A. C., "Stroboscopic ultrahigh-resolution full-field optical coherence tomography," Opt. Lett. 30, 1351-1353 (2005).

[18] Dunsby, C., Gu, Y. and French, P., "Single-shot phase stepped wide-field coherence gated imaging," Opt. Express, 11, 105-115 (2003).

[19] Hrebesh, M. S., Dabu, R. and Sato, M., "In vivo imaging of dynamic biological specimen by real-time single-shot full-field optical coherence tomography," Opt. Comm. 282, 674-683 (2009).

[20] Sacchet, D., Brzezinski, M., Moreau, J., Georges, P. and Dubois, A., "Motion artifact suppression in full-field optical coherence tomography," Appl. Opt. 49, 1480-1488 (2010).

[21] Schausberger, S. E., Heise, B., Bernstein, S. and Stifter, D., "Full-field optical coherence microscopy with Riesz transform-based demodulation for dynamic imaging," Opt. Lett. 37, 4937-4939 (2012).

[22] Karamata, B., Lambelet, P., Laubscher, M., Salathé, R. P. and Lasser, T., "Spatially incoherent illumination as a mechanism for cross-talk suppression in wide-field optical coherence tomography," Opt. Lett. 29, 736-738 (2004).

[23] Dubois, A., Moneron, G., Grieve, K. and Boccara, A.C., "Three-dimensional cellular-level imaging using full-field optical coherence tomography," Phys. Med. Biol. 49, 1227-1234 (2004).

[24] Ogien, J. and Dubois, A., "High-resolution full-field optical coherence microscopy using a broadband light-emitting diode," Opt. Express 24, 9922-9931 (2016).

[25] Dubois, A., [Handbook of full-field optical coherence microscopy: technology and applications], Chapter 1, 1-40, Pan Stanford Publishing, Singapore (2016).
[26] Dalimier, E., Bruhat, A., Grieve, K., Harms, F., Martins, F. and Boccara, A. C., "High resolution in-vivo imaging of skin with full field optical coherence tomography," Proc. SPIE 8926, 8926P (2014).